Anomalous Protein Diffusion in Living Cells as Seen by Fluorescence Correlation Spectroscopy

Matthias Weiss, Hitoshi Hashimoto, and Tommy Nilsson
Cell Biology and Cell Biophysics Programme, European Molecular Biology Laboratory, 69117 Heidelberg, Germany

ABSTRACT We investigate the challenges and limitations that are encountered when studying membrane protein dynamics in vivo by means of fluorescence correlation spectroscopy (FCS). Based on theoretical arguments and computer simulations, we show that, in general, the fluctuating fluorescence has a fractal dimension $D_0 \geq 1.5$, which is determined by the anomality α of the diffusional motion of the labeled particles, i.e., by the growth of their mean square displacement as $(\Delta x)^2 \sim t^\alpha$. The fractality enforces an initial power-law behavior of the autocorrelation function and related quantities for small times. Using this information, we show by FCS that Golgi resident membrane proteins move subdiffusively in the endoplasmic reticulum and the Golgi apparatus in vivo. Based on Monte Carlo simulations for FCS on curved surfaces, we can rule out that the observed anomalous diffusion is a result of the complex topology of the membrane. The apparent mobility of particles as determined by FCS, however, is shown to depend crucially on the shape of the membrane and its motion in time. Due to this fact, the hydrodynamic radius of the tracked particles can be easily overestimated by an order of magnitude.

INTRODUCTION

The diffusive behavior plays a crucial role in determining the activity and function of molecules, e.g., in diffusion-limited reactions and the formation of cellular patterns (Murray, 1993). For membrane proteins, diffusive motion enables segregation into subdomains and subsequently transport intermediates in the endoplasmic reticulum (ER) and Golgi apparatus (for reviews see Antonny and Shekman, 2001; Storrie and Nilsson, 2002). To better understand such processes, one wishes not only to determine the overall behavior of the proteins but also to gain detailed knowledge about their state. For example, is the protein of interest transiently part of an oligomeric complex (Nilsson et al., 1994), a lipid raft (Simons and Ikonen, 2000), and/or does it associate with the cytoskeleton (Yamaguchi and Fukuda, 1995)? Evidence for such interactions can be obtained by assessing the detailed diffusive behavior of the protein. Diffusion will be slower if associating transiently with the cytoskeleton and/or being partly in a lipid raft or a larger complex. It is likely that proteins experience more than one type of interaction in vivo, and if the interacting partners have a lower mobility than the protein in study, it will seem to take rests between times of free diffusional motion. As the resting times associated with these interactions are likely to vary widely, subdiffusive motion may be observed (Nagle, 1992; Saxton, 2001), i.e., the protein shows a time-dependent mobility and diffusion coefficient $D(t)$.

Although it is likely that proteins experience multiple types of interactions resulting in subdiffusive behavior, it has proved difficult to determine this experimentally. Though with confocal bleaching techniques, i.e., fluorescence recovery after photobleaching (FRAP), a detection of anomalous diffusion is in principle possible (Saxton, 2001), this elusive information is often distorted by fluctuations in the recovery curve. Moreover, due to the complexity of the membrane morphology, anomalous diffusion can arise as a pure geometrical effect even if the particle diffuses normally (Sbalzarini, Mezzacasa, Helenius, and Koumoutsakos, unpublished). An alternative to FRAP is fluorescence correlation spectroscopy (FCS), which provides more local information and yields a higher temporal resolution at the level of single molecules (Rigler and Elson, 2001). However, even with FCS it is a challenge to detect and extract subdiffusive motion reliably (Schwille et al., 1999a,b).

Besides the issue of anomalous diffusion, the precise determination of mobilities is of high interest for the elucidation of biological questions, as it often serves as a key parameter for pattern formation (Murray, 1993). It was hypothesized, for example, that Golgi resident membrane proteins show complex formation upon reaching the Golgi (Nilsson et al., 1993, 1994). Similarly, unfolded membrane proteins in the ER were predicted to associate with a network of chaperones, which should lead to a lower mobility (Tatu and Helenius, 1997). Both questions have in part been addressed by FRAP in vivo (Cole et al., 1996; Nehls et al., 2000), and based on the apparent mobilities of the investigated proteins, it was argued that neither of the above hypotheses was correct. However, it remains open if FRAP or FCS can really assess the mobility in enough detail to definitely answer the posed questions.

Here, we provide evidence that anomalous diffusion manifests itself as fractal fluctuations of the fluorescence $F(t)$, i.e., the fractal dimension D_0 of $F(t)$ depends on the anomality of the diffusion. As a consequence, the autocorrelation function of $F(t)$ and the variance of fluorescence

Submitted October 30, 2002, and accepted for publication February 11, 2003.

Address reprint requests to Matthias Weiss, Cell Biology and Cell Biophysics Programme, European Molecular Biology Laboratory, Meyerhofstr. 1, 69117 Heidelberg, Germany. Tel.: +49-6221-387-408; Fax: +49-6221-387-512; E-mail: mweiss@embl-heidelberg.de.

0006-3495/03/06/4043/10 $2.00

increments show a power-law behavior for small times. We confirm this by computer simulations and employ this knowledge to evaluate experimental FCS curves of membrane proteins in the ER and Golgi apparatus, in vivo. We find that all tested proteins move subdiffusively, but have different degrees of anomality. Secondly, we show that the shape of the membrane does not induce subdiffusive behavior even if the curvature changes with time, but it does affect the apparent mobility. In fact, the uncertainty in the mobility is typically big enough to prevent a monomeric membrane protein to be distinguished from a cluster consisting of several hundred monomers.

METHODS

Theoretical background of FCS

The basic idea of FCS is to monitor the fluctuating number of labeled particles in a confocal laser spot with an intensity profile that is commonly approximated by a three-dimensional Gaussian, i.e.,

$$I(\mathbf{r}) = I_0 \exp\{-2(x^2 + y^2 + (z/S)^2)/r_0^2\}. \quad (1)$$

The characteristic width of the spot in z direction is typically S-fold larger than the width r_0 in xy direction, where $S \approx 5 - 10$ (Rigler and Elson, 2001). The density $n(\mathbf{r},t)$ of labeled particles at a point $\mathbf{r}$ in the focus fluctuates as particles are subject to diffusion, yielding the time-averaged autocorrelation function

$$\langle n(\mathbf{r},t)n(\mathbf{r}',t+\tau)\rangle_t = \int\int n(\mathbf{r},t)\mathcal{G}(\mathbf{r}',\mathbf{r}'',\tau)n(\mathbf{r}'',t)d\mathbf{r}''\,dt.$$

Here, we have made use of the Greens function $\mathcal{G}(\mathbf{r},\mathbf{r}',\tau)$ of the diffusion equation, i.e., the propagator of the density $n(\mathbf{r},t)$ and the integrations run over all times and the whole space, respectively. Separating the fluctuations and the average density by $n(\mathbf{r},t) = \bar{n} + \delta n(\mathbf{r},t)$ and assuming the fluctuations to have zero mean and to be uncorrelated at different spatial positions at any time point yields: $\langle n(\mathbf{r},t)n(\mathbf{r}',t+\tau)\rangle_t = \bar{n}^2 + \mathcal{G}(\mathbf{r},\mathbf{r}',\tau)$. As the measurable signal is the total fluorescence in the confocal volume $F(t) = \int I(\mathbf{r})n(\mathbf{r},t)d\mathbf{r}$, one obtains from that and Eq. 1 the autocorrelation function of the fluorescence signal

$$\langle F(t)F(t+\tau)\rangle_t = A + \int\int I(\mathbf{r})I(\mathbf{r}')\mathcal{G}(\mathbf{r},\mathbf{r}',\tau)d\mathbf{r}\,d\mathbf{r}',$$

with $A = \left(\bar{n}\int I(\mathbf{r})d\mathbf{r}\right)^2$. Here, both integrals are taken over the whole space and A is a constant that depends on $\bar{n}$, I_0, and properties of the fluorophore. As we are only interested in the decay of the correlation, we define by

$$C(\tau) = \int\int I(\mathbf{r})I(\mathbf{r}')\mathcal{G}(\mathbf{r},\mathbf{r}',\tau)d\mathbf{r}\,d\mathbf{r}' \quad (2)$$

the autocorrelation function of the fluorescence fluctuations, which decays to zero as $\tau \to \infty$.

We note that the decay of $C(\tau)$ is essentially determined by the Greens function $\mathcal{G}$ of the diffusion equation. Denoting by g_{ij} the metric of the (curved) manifold of diffusion in Cartesian coordinates, its inverse by g^{ij} and letting $\sqrt{g} = \sqrt{\det(g_{ij})}$, the diffusion equation reads in general

$$\frac{\partial n}{\partial t} = \frac{D}{\sqrt{g}}\frac{\partial}{\partial x^i}\left(\sqrt{g}g^{ij}\frac{\partial n}{\partial x^j}\right), \quad (3)$$

where we have used a covariant notation and the Einstein summing convention (Misner et al., 1973). The Greens function $\mathcal{G}(\mathbf{r},\mathbf{r}',t)$ satisfies Eq. 3 with the constraint $\mathcal{G}(\mathbf{r},\mathbf{r}',t=0) = \delta(\mathbf{r} - \mathbf{r}')$ and can be calculated analytically only in rare cases, e.g., for diffusion on the xy plane perpendicular to the optical axis. In that case the metric is particularly simple ($g_{ij} = \delta_{ij}$, $i, j = 1,2$) and one obtains from Eq. 3 the familiar two-dimensional diffusion equation with the Greens function $\mathcal{G}(\mathbf{r},\mathbf{r}',t) = \exp\{-|\mathbf{r} - \mathbf{r}'|^2/(4Dt)\}/(4\pi Dt)$. With that, the integrals in Eq. 2 can be solved analytically, yielding the well-known autocorrelation function

$$C(\tau) = \frac{B}{1 + \tau/\tau_D}, \quad (4)$$

where $\tau_D = r_0^2/(4D)$ is the diffusive time and B is a constant that, in general, includes the average number of molecules in the focus and properties of the fluorophore. In case of two different, noninteracting kinds of particles labeled with the same fluorophore but having diffusive times $\tau_D^{(1)}$, $\tau_D^{(2)}$ and fractions f, $1 - f$, respectively, the total correlation curve is simply the sum of two individual curves (Schwille et al., 1999a):

$$C(\tau) = \frac{fB}{1 + \tau/\tau_D^{(1)}} + \frac{(1-f)B}{1 + \tau/\tau_D^{(2)}}. \quad (5)$$

This expression may easily be extended to an arbitrary number of populations.

Monte Carlo simulations of anomalous and constrained diffusion

In all simulations, we have fixed the characteristic radius of the confocal spot to $r_0 = 0.3$ μm in the xy plane and chose the laser intensity to be $I_0 = 1$. The radius of the confocal volume in z direction was chosen to be fivefold bigger ($S = 5$), which is a typical value (Rigler and Elson, 2001). To test the fractality of $F(t)$, we initially distributed 100 particles randomly on a two-dimensional plane (edge length $L = 2.1$ μm) with periodic boundaries, perpendicular to the optical axis. The erratic motion was simulated using the forward integration of the Langevin equation, i.e., $x(t + dt) = x(t) + \xi(dt)$, with time increments $dt = 1$ μs. As a model for subdiffusive motion, we have chosen to calculate the spatial increments $\xi(dt)$ in x and y direction via the Weierstrass-Mandelbrot function (Berry and Lewis, 1980; Saxton, 2001)

$$W(t) = \sum_{n=-\infty}^{\infty} \frac{\cos(\phi_n) - \cos[\gamma^n t^* + \phi_n]}{\gamma^{nH}}. \quad (6)$$

Here, ϕ_n are random phases in the interval $[0,2\pi]$, $\gamma > 1$ is an irrational number, $t^* = 2\pi t/t_{max}$ is connected to the maximum length t_{max} of the desired time series, and $H = \alpha/2$ is the Hurst coefficient leading to a growth of the particles' mean square displacement as $(\Delta x)^2 \sim t^\alpha$. In accordance with Saxton (2001), we chose $\gamma = \sqrt{\pi}$ and restricted the sum to the terms $n = -8, \ldots, 48$. The increments $\xi(dt) = W(t + dt) - W(t)$ were scaled to match the desired values of the transport coefficient Γ. For the chosen $\alpha = 1,0.7,0.5$ and $\Gamma = 57/s,50/s^{0.7},39/s^{0.5}$, we took 10 time series of length $t_{max} = 5$ s for averaging.

Fractal analysis was performed by using a box-counting algorithm, i.e., the curve $F(t)$ is covered with squares of length τ and the number of filled boxes $\chi(\tau)$ is counted. This quantity shows a scaling $\chi(\tau) \sim \tau^{-D_0}$. In contrast, $C(\tau)$ and $v(\tau)$ were calculated directly from $F(t)$. While $v(\tau)$ in the simulations was monotonically increasing with τ, the experimental curve had an offset $v_0 = v(\tau \to 0) > 0$ due to the stochastic nature of the emission of the fluorophore. Consequently we subtracted this offset and analyzed $v(\tau) - v_0$.

Monte Carlo simulations of diffusion on surfaces with nonzero curvature, defined by $\phi(\mathbf{r}) = 0$, were performed using the algorithm proposed in (Hołyst et al., 1999). In brief, we calculated the local Cartesian frame of the tangential surface $(\mathbf{r} - \mathbf{r}_0)\cdot\nabla\phi(\mathbf{r}_0) = 0$ at the position $\mathbf{r}_0$ of every particle. We then drew Gaussian random numbers with variance $2D\Delta t$ for the in-plane stochastic movement in each direction of the local Cartesian frame. The resulting vector $\mathbf{r}_1$ was projected back to the surface $\phi = 0$ yielding the

new position $\mathbf{r}_2 = \mathbf{r}_1 - \phi(\mathbf{r}_1)\nabla\phi(\mathbf{r}_1)/|\nabla\phi(\mathbf{r}_1)|$. For sufficiently small Δt, the erratic movement of the particles is bound to the surface (Hołyst et al., 1999). In all simulations we used $I_0 = 1$, $r_0 = 0.3$ μm, 100 particles, $\Delta t = 10^{-7}$ s, $D = 1$ μm^2/s, and $S = 5$.

Cell culture, fluorescence microscopy, and FCS

Stable HeLa cell lines were constructed by transfection with plasmid DNA encoding the trans-membrane proteins GalNAc-T2 or p24β1 fused to green fluorescent protein (GFP) and yellow fluorescent protein (YFP), respectively, and selected for using G418 as described previously (Storrie et al., 1998). Cells were grown in Dulbecco's modified Eagle's medium with 10% fetal calf serum, 100 μg/ml penicillin, 100 mg/ml streptomycin, and 10 mM glutamine (Gibco, Eggenstein, Germany). HeLa cells expressing GalT(GFP) were obtained by microinjecting purified pGalT plasmid (concentration 50 ng/ml) into cell nuclei using an Eppendorf microinjection system (Eppendorf, Hamburg, Germany) and Cascade blue dextran (Molecular Probes, Eugene, OR) as a coinjection marker.

FCS measurements were carried out with a commercial instrument (ConfoCor II, Carl Zeiss, Jena, Germany), combining a laser scanning and an FCS unit. The used objective was an Apochromat 40x/1.2 W. With this setup, a spot on a previously scanned image of a cell could be selected for the FCS measurement. The spatial resolution is ~0.5 μm, corresponding to an average spot size of 0.3 μm. GFP-tagged proteins were illuminated at 488 nm and detected with a bandpass filter (505–550 nm). To reduce the unavoidable deviations of the optical volume from a Gaussian form, we used very low laser intensities in the range 40–100 μW. As can be seen from Fig. 7 *a*, in this range the approximation of a Gaussian confocal volume is well in agreement with previous reports for the ConfoCor II (T. Jankowski and R. Janka, 2001). For higher laser powers, however, the deviations become much stronger (Fig. 7 *b*), in agreement with Hess and Webb (2002). More details on this issue are given in the Discussion. The pinhole for all shown measurements was 1 Airy unit (70 μm) unless stated otherwise. Calibration of the diffusional timescale was done with GFP in water ($D \approx 87$ μm^2/s) (Wachsmuth et al., 2000). For the measurements on GFP-tagged proteins, 10–20 time series of 10 s were recorded with a time resolution of 1 μs and then superimposed for fitting. Measurements on the Golgi were preceded by bleaching to decrease the fluorescence below the saturation value of the detectors.

RESULTS

Anomalous diffusion and fractal fluorescence fluctuations

The principle idea of modern FCS is to monitor the total fluorescence $F(t)$ arising due to the fluctuating density of labeled particles in a confocal laser spot of width r_0 (see Methods). These fluctuations are a consequence of the particles' (anomalous) diffusive motion in and out of the confocal volume, which has a volume of ~1 fl. Anomalous diffusion implies that the particles' mean square displacement grows asymptotically as $(\Delta x)^2 = 4\Gamma t^\alpha$, $\alpha \le 1$, and the autocorrelation function for particles moving on a plane perpendicular to the optical axis then reads in general

$$C(\tau) = \frac{B}{1 + \Gamma\tau^\alpha/(4r_0^2)}. \quad (7)$$

In fact, Eq. 7 is a generalization of Eq. 4, which describes the special case of normal diffusion ($\alpha = 1$). The transport coefficient Γ has the dimension of an area per fractional time (μm^2/s$^\alpha$), and one can define a time-dependent diffusion coefficient by $D(t) = \Gamma t^{\alpha-1}$. This expression converges to a constant $D = r_0^2/(4\tau_D)$ for normal diffusion ($\alpha \to 1$), where τ_D, defined by $C(\tau) = B/2$, is the diffusive time. Fitting the experimental FCS curve with Eq. 7 therefore yields the local transport coefficient Γ and the degree of anomality α.

To overcome the reported ambiguity that experimental FCS curves can be fitted successfully with Eq. 7 and expressions that describe coexisting populations of proteins with different mobilities (Schwille et al., 1999a,b) (cf. Eq. 5), we took a closer look at the fluctuations of the fluorescence time series $F(t)$, i.e., its basic statistical properties. Restricting the correlation analysis to the regime $\Gamma\tau^\alpha \ll 4r_0^2$, one obtains from Eq. 7 $C(\tau) \sim$ const. $- \tau^\alpha$. This scaling is very similar to the characteristic behavior found for a certain class of stochastic processes known as fractional Brownian motion (Mandelbrot and Ness, 1968). These processes are characterized by the above asymptotic algebraic autocorrelation decay, a growth of the variance of (fluorescence) increments $v(\tau) = \langle (F(t) - F(t + \tau))^2 \rangle_t \sim \tau^\alpha$ and a fractal dimension $D_0 = 2 - \alpha/2$ of the curve $F(t)$. These signatures of fractional Brownian motion have been found and characterized in detail, e.g., in conductance fluctuations of mesoscopic samples in solid-state physics (Hufnagel et al., 2001; Maspero et al., 2000). From the analogy of fractional Brownian motion and the small-τ limit of Eq. 7, we conclude that the fluorescence time series $F(t)$ taken in FCS measurements should exhibit a fractal dimension $D_0 = 2 - \alpha/2$ on short timescales and we anticipate an increase $v(\tau) = \langle (F(t) - F(t + \tau))^2 \rangle_t \sim \tau^\alpha$ for the variance of the fluorescence increments. In fact, the scaling $v(\tau) \sim t^\alpha$ is intimately related to the initial decay of $C(\tau)$ via $v(\tau) =$ const. $- C(\tau)$ and therefore it is a sensitive measure for the anomality when restricting the analysis to small times. A fractal analysis of $F(t)$ therefore should provide the desired informations D_0 and α about the diffusive process without having to fit the entire autocorrelation function $C(\tau)$.

We have tested our expectations quantitatively with the help of Monte Carlo simulations using different levels of subdiffusion (see Methods). We simulated (sub)diffusive motion of particles on a plane for $\alpha = 1$, 0.7, 0.5 and monitored the fluorescence $F(t)$ arising from a Gaussian intensity profile. A fractal analysis of this signal confirmed the fractality of $F(t)$ ($D_0 = 2 - \alpha/2$), the relation $v(\tau) \sim \tau^\alpha$, whereas $C(\tau)$ was perfectly described by Eq. 7 (see Fig. 1).

We emphasize that the dimension of the sample on which the particles diffuse, as well as the number of different components, enter in the above arguments only as prefactors, which does not affect the scaling. Since only α determines the fractal dimension D_0, our approach should thus be capable of reliably extracting α for one-, two-, and three-dimensional motion with an arbitrary number of different components.

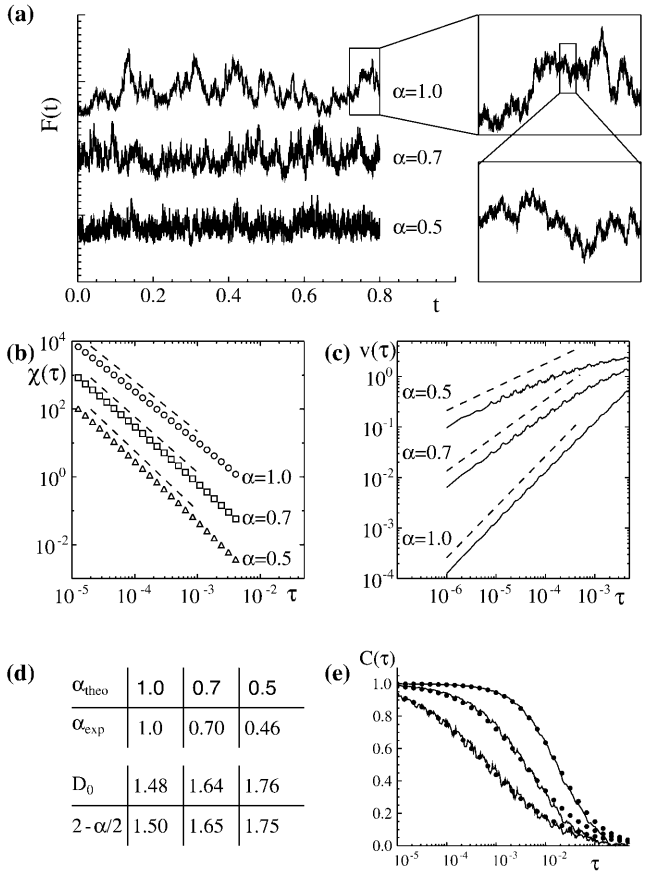

(d)			
α_{theo}	1.0	0.7	0.5
α_{exp}	1.0	0.70	0.46
D_0	1.48	1.64	1.76
$2-\alpha/2$	1.50	1.65	1.75

FIGURE 1 Confirmation of fractal fluorescence fluctuations. (*a*) Fluorescence $F(t)$ for $\alpha = 1.0, 0.7, 0.5$ (*from top*), with magnifications to expose the self-similarity. (*b*) The results of a box-counting algorithm (see Methods) applied to $F(t)$ (*symbols*) agrees with the anticipated scaling relation $\chi(\tau) \sim \tau^{-D_0}$ (*dashed lines*). (*c*) The variance of the fluorescence increments (*full lines*) shows the expected behavior $v(\tau) \sim \tau^{\alpha}$ (*dashed lines*). (*d*) The theoretically expected values α_{theo} and $2 - \alpha/2$ agree nicely with the results α_{exp} and D_0 obtained from the fractal analysis. (*e*) The autocorrelation curves $C(\tau)$ (*full lines*) are well described by Eq. 7 with the appropriate α (*symbols*). All times t, τ are in units of seconds.

Anomalous diffusion of membrane proteins in vivo

We next tested the fractal analysis as a method to investigate anomalous diffusion of membrane proteins in vivo. Three Golgi resident enzymes tagged with GFP, *N*-acetylgalactosyltransferase 2 (GalNAc-T2(GFP)), 1,4β-galactosyltransferase GalT(GFP), and p24β1(YFP) were monitored both in the ER and in the Golgi. As only ~5–10% of these proteins localize to the ER (Storrie et al., 1998) (see also Fig. 2, *a–c*), we could be certain to meet the low-fluorescence situation typically anticipated in FCS measurements. From the offset of the autocorrelation curves in the ER, we estimated the average number of proteins in the focus in all cases to be <30. For the Golgi, we performed a prebleach before the measurement to avoid saturation of the FCS detector.

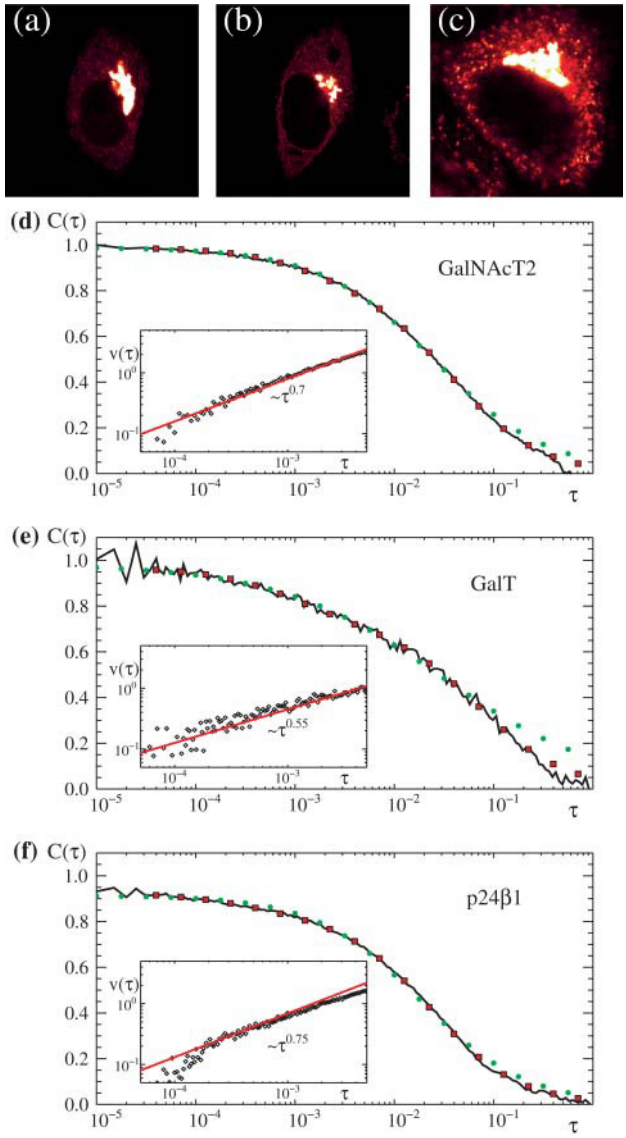

FIGURE 2 Anomalous diffusion of membrane proteins in the ER, in vivo. (*a–c*) HeLa cells expressing GalNAc-T2(GFP), GalT(GFP), and p24β1(YFP), respectively. A pronounced Golgi and a small ER pool of the labeled proteins are visible. (*d*) Autocorrelation function $C(\tau)$ for GalNAc-T2(GFP) in the ER (*black*), which is equally well described by a two-component expression (*green circles*) and anomalous diffusion (Eq. 7) with $\alpha = 0.75$, $\Gamma = 0.2\ \mu m^2/s^{0.75}$ (*red squares*). Inset: as anticipated, the variance of the increments $v(\tau) \sim \tau^{\alpha}$ follows a power law with $\alpha \approx 0.7$, in agreement with the result obtained by fitting $C(\tau)$ with Eq. 7. (*e*) Same for GalT(GFP) in the ER with $\alpha = 0.55$, $\Gamma = 0.08\ \mu m^2/s^{0.55}$. Inset: the variance of the increments confirms the anomalous diffusion ($v(\tau) \sim \tau^{0.55}$). (*f*) Same for p24β1(YFP) in the ER with $\alpha = 0.8$, $\Gamma = 0.3\ \mu m^2/s^{0.8}$. Inset: the variance of the increments confirms the anomalous diffusion ($v(\tau) \sim \tau^{0.75}$). All times τ are in units of seconds.

As can be seen from Fig. 2 *d*, the normalized autocorrelation function $C(\tau)$ for GalNAc-T2 is described equally well by Eq. 7 for anomalous diffusion and by an expression describing the coexistence of two populations with different mobilities (Methods, Eq. 5). However, these fits describe entirely different behaviors: whereas the first

predicts a time-dependent diffusion coefficient $D(t) = 0.2/t^{0.25}$ $\mu m^2/s^{0.75}$ as $\alpha = 0.75$, the second predicts two GalNAc-T2 populations having diffusion constants $D_1 = 0.3$ $\mu m^2/s$ and $D_2 = 7$ $\mu m^2/s$. Similar to earlier reports (Schwille et al., 1999a,b), one cannot determine which of the two scenarios is actually underlying the experimental data.

Due to the low level of fluorescence, the scaling of $\chi(\tau)$ did not extend over a broad enough range in τ to allow for a reliable estimate of D_0 and α. Therefore, the scaling of $v(\tau)$ for small τ was the only way to test for anomalous diffusion. As will become clear in the next section, it provides nevertheless a more valuable tool to determine the anomality α than fitting the entire function $C(\tau)$. Indeed, we found a scaling $v(\tau) \sim \tau^{\alpha}$, $\alpha = 0.7 \pm 0.05$ (Fig. 2, *inset*) that agrees well with the fitting of the entire $C(\tau)$ with Eq. 7 over four orders of magnitude in τ. We confirmed this result for different cells and various ER sites. From this we conclude that GalNAc-T2 actually moves subdiffusively in the ER.

A close look at the diffusion constant of proteins in membranes (Saffman and Delbrück, 1975), i.e., $D = k_BT(\ln\{h\eta_m/\eta_cR\} - 0.5772)/(4\pi\eta_m h)$ supports this conclusion: estimating the radius of the membrane spanning domain of GalNAc-T2 to be $R \approx 1$ nm (slightly bigger than the size of a single α-helix), the thickness of the membrane to be $h \approx 6$ nm and assuming the membranous and cytosolic viscosities to be $\eta_m \approx 0.15$ kg m/s and $\eta_c \approx 0.003$ kg m/s, the ratio $D_2/D_1 = 23.5$ obtained from Fig. 2 *d* by fitting with a multiple-component expression implies a hydrodynamic radius $R \approx 135$ nm of the second component. In fact, this particle then had to consist of more than 10^4 GalNAc-T2 monomers, which appears somewhat large.

To rule out that the observed anomalous behavior was a special feature of GalNAc-T2, we also tested the ER pool of GalT and p24β1, two integral membrane proteins that localize preferentially to the late and early Golgi apparatus, respectively (Fig. 2, *b* and *c*). Again we found anomalous diffusion for these proteins (Fig. 2, *d* and *e*). Whereas the anomality for GalT ($\alpha = 0.5 \pm 0.05$) appeared to be even stronger than for GalNAc-T2, p24β1 showed a slightly less subdiffusive behavior ($\alpha = 0.8 \pm 0.05$). We next monitored the mobility of GalNAc-T2 and p24β1 in the Golgi apparatus. As shown in Fig. 3, the same degrees α of subdiffusiveness were also observed in the Golgi.

To investigate the reason for the observed subdiffusion, we tested different conditions while monitoring the membrane proteins in vivo: a shift in temperature from 37°C to room temperature (23°C) did not seem to alter the anomalous diffusion, although one might suspect this due to possible phase transitions in the membrane. Most likely, nothing crucial in terms of lipids took place, which is also indicated by the fact that the exocytic pathway works efficiently at room temperature. Blocking protein synthesis by cyclohexamide (incubation for 2 h before measurement) also did not affect the anomalous diffusion. This indicates that new, partially unfolded proteins that associate with the ER quality control machinery are not the ones that give the major contribution to the anomalous FCS signal. Removal of microtubules by applying the drug nocodazole also showed no effect, which rules out that the reported binding to microtubules (Yamaguchi and Fukuda, 1995) plays a major role. Inactivating the COPII machinery by a Sar1^{dn} GDP-restricted mutant that blocks export from the ER also did not alter the obtained results. We speculate that the most likely explanation for the observed subdiffusion is a continuous time random walk, i.e., a random walk with rests due to transitional bindings in between. Dicing the resting times according to an algebraic distribution, one can obtain any value of $0 < \alpha < 1$ (Nagle, 1992; Saxton, 2001). Although obstacles on the membrane will also contribute to subdiffusive motion (Saxton, 2001), this can reduce the anomality even at the percolation threshold only to $\alpha \approx 0.7$, which is bigger than the observed value $\alpha = 0.5$ for GalT. The continuous time random walk may be caused by transient bindings to larger proteins, e.g., the UDP-glucose transporter or specialized protein-lipid domains (Simons and Ikonen, 2000).

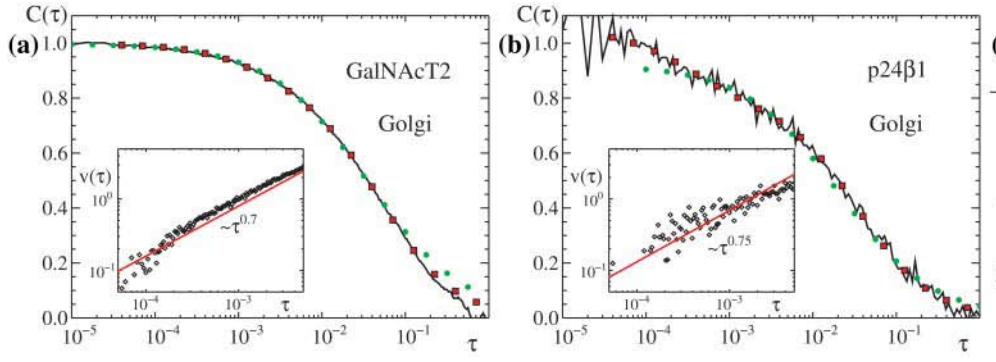

FIGURE 3 Anomalous diffusion of membrane proteins in the Golgi, in vivo. (*a*) Same as in Fig. 2 *d* for GalNAc-T2 in the Golgi (*full black*) yielding $\alpha = 0.75$, $\Gamma = 0.15$ $\mu m^2/s^{0.75}$ (*red squares*). (*b*) Same as in Fig. 2 *f* for p24β1 in the Golgi (*full black*) yielding $\alpha = 0.75$, $\Gamma = 0.2$ $\mu m^2/s^{0.7}$ (*red squares*). (*c*) The table summarizes the results for the degree of anomality α for the different proteins and conditions. All times τ are in units of seconds.

Influence of the membrane shape on the apparent mobility

Whereas we could confirm the degree of anomality α for integral membrane proteins under different conditions, the transport coefficient Γ showed considerable variations. We reasoned that this was most probably caused by the local morphology of the membrane. The effect of geometrical constraints on FCS has so far not been a point of major considerations. Only the special case of three-dimensional diffusion between fixed, reflecting boundaries has been studied in some detail (Gennerich and Schild, 2000). For FCS on membranes, however, most experimental data are still evaluated with the simple expression Eq. 4. In the following, we restrict ourselves to normal diffusion and we first turn to the easiest nontrivial extension of a plane membrane perpendicular to the optical axis (Eq. 4), i.e., a tilted plane. Without loss of generality, we assume that the tilted plane emerges by rotating the xy plane by an angle θ around the y axis (a shift with respect to the focus will only affect the prefactor B in which we are not interested). The metric for this tilted plane in Cartesian coordinates is given by $g_{11} = 1 + \tan^2(\theta)$, $g_{22} = 1$, $g_{12} = g_{21} = 0$, from which one obtains the autocorrelation function

$$C(\tau) = \frac{B}{\sqrt{1+\tau/\tau_D}\sqrt{1+\xi(\theta)\tau/\tau_D}} \tag{8}$$

$$\xi(\theta) = \cos^2(\theta) + \sin^2(\theta)/S^2,$$

which converges to Eq. 4 in the limit $\theta \to 0$. Some representative examples of Eq. 8 for various θ are shown in Fig. 4 *a*. In real applications, however, one may not know if and how much a membrane is actually tilted. Fitting $C(\tau)$ then naively with Eq. 4 results in an overestimation of τ_D, which may be as high as 2.5-fold (Fig. 4 *a*, *inset*).

Even worse, in living cells the membranes themselves are subject to fluctuations, reformation, and active transport. Consequently, the angle θ may be a function of time. We have simulated this by changing θ periodically by a factor $\cos(\omega t)$ with $\omega = 0.2\pi, 2\pi, 20\pi$ Hz (Fig. 4 *b*). The obtained curves are well described by the angle-averaged expression of Eq. 8, i.e.,

$$\langle C(\tau,\theta)\rangle_\theta = \frac{BK\{\tau(S^2-1)/[S^2(\tau_D+\tau)]\}}{1+\tau/\tau_D}, \tag{9}$$

where K is the complete elliptic integral of first order. Fitting the numerical curves with Eq. 4, however, results in a 1.5-fold overestimation of τ_D.

We speculated that diffusion on curved surfaces could yield even higher overestimations of τ_D, when fitting naively with Eq. 4. We concentrated on hyperbolic and parabolic surfaces as the easiest examples of a 2D surface with nonzero curvature defined by

$$z = \sigma\frac{x^2}{a^2} - \frac{y^2}{b^2}, \tag{10}$$

with $\sigma = +1$ and $\sigma = -1$, respectively. In these cases all components of the metric tensor in Cartesian coordinates are algebraic functions of x,y and thus solving Eq. 3 to obtain $\mathcal{G}(\mathbf{r},\mathbf{r}',t)$ becomes very complicated. As we have not been able to derive $C(\tau)$ analytically, we performed Monte Carlo simulations to gain some insight in the behavior of the correlation decay. For the sake of simplicity, we have set $a = b$ and investigated the autocorrelation function for various a. In Fig. 5 *a*, the result for the hyperbolic surface is shown in comparison to $C(\tau)$ derived from Eq. 4 when inserting the mobility used in the simulations. Obviously an overestimation of τ_D up to a factor 4.5 with decreasing a is observed and the shape of the autocorrelation function seems to be stretched. Therefore, it was tempting to compare the curves to Eq. 7, which yields a reasonable fit. It thus seems as if the degree of subdiffusiveness α depended on a and tends to unity for $a \gg r_0$. A fractal analysis of the fluorescence, i.e., using a box-counting algorithm (Maspero et al., 2000) and inspecting the small time limit of $v(\tau)$, does not yield any hint that anomalous diffusion produces the observed $C(\tau)$, as anticipated from the definition of the simulation. This is a nice example, where the fractal analysis, and in particular the behavior of $v(\tau)$ for small times, can decide whether

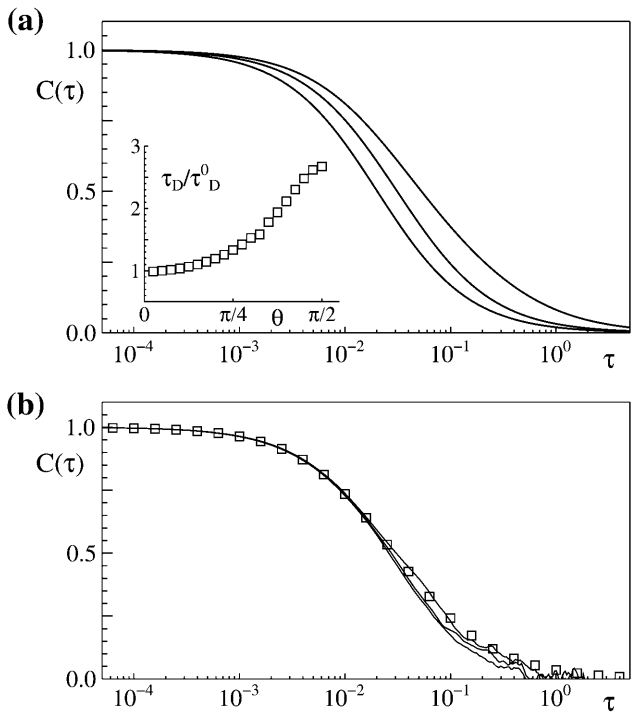

FIGURE 4 (*a*) Autocorrelation curves $C(\tau)$ for a tilted plane enclosing an angle $\theta = 0,\pi/3,\pi/2$ with the xy plane (*curves from left to right*). The inset shows the error ratio τ_D/τ_D^0 of the diffusive time τ_D as obtained by fitting $C(\tau)$ naively with Eq. 4 and the theoretical value $\tau_D^0 \approx 0.02$ ms as a function of θ. (*b*) Tilting the plane periodically with 0.2–20 Hz in the interval $\theta \in [-\pi/3, \pi/3]$ is well described by the angle-averaged correlation function (Eq. 9, *symbols*) and yields an error ratio $\tau_D/\tau_D^0 \approx 1.5$. All times τ are in units of seconds.

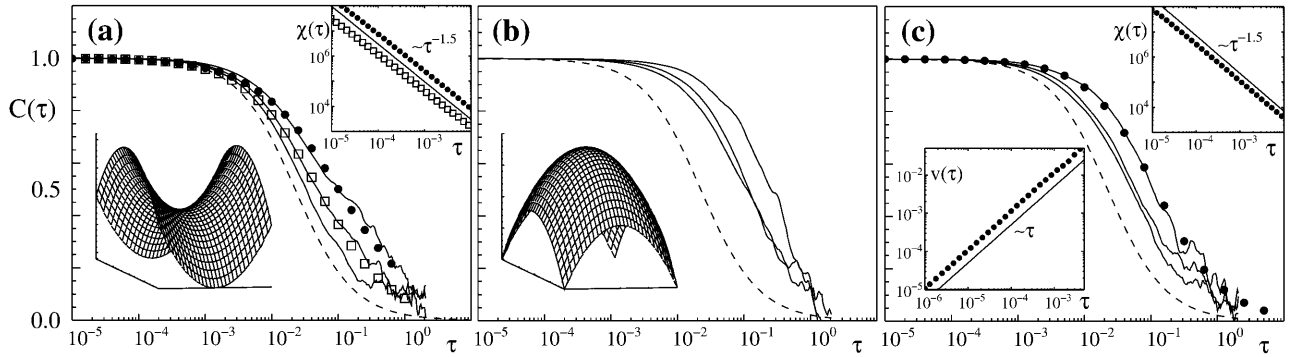

FIGURE 5 (*a*) Autocorrelation curves for a hyperbolic surface according to Eq. 10 (*inset lower left*) with $a = r_0/2, r_0, 2r_0$ (*full lines, from right*). Compared to Eq. 4 when using the mobility used in the simulation (*dashed*), the decay is slowed down by a factor 4.5, 2.3, and 1.1, respectively. The numerical curves seem to be well described by Eq. 7, implying anomalous diffusion with $\alpha = 0.7$ (*dots*) and $\alpha = 0.8$ (*squares*), respectively. This purely geometry-induced subdiffusion is ruled out by a fractal analysis (*inset*, *upper left*), which yields $\alpha = 1 \Rightarrow D_0 = 1.5$ as used in the simulations. (*b*) Same as in *a* for a parabolic surface (*inset*). The underestimation of the mobility is 10-fold ($a = r_0/2$), 5.2-fold ($a = r_0$), and 4.8-fold ($a = 1.4r_0$), respectively, and no signs of subdiffusive motion are observed. (*c*) When smoothly interpolating between parabolic and hyperbolic surfaces by varying σ in Eq. 10 stochastically, a slower decay of $C(\tau)$ is observed (*left to right*: slower variation of σ). The influence of the hyperbolicity seems to induce anomalous diffusion as $C(\tau)$ is described well by Eq. 7 (*symbols*). However, a fractal analysis reveals this as mistaken and verifies the normal diffusion (*insets*). All times τ are in units of seconds.

anomalous diffusion is observed or if it is rather an effect induced by geometry.

For parabolic surfaces, the underestimation of the mobility is even more pronounced (Fig. 5 *b*), whereas the curves are similar to Eq. 4 in their decay behavior. In fact, the mobility can be underestimated easily by an order of magnitude. Again, the fractal analysis did not yield any hint of anomalous diffusion, as anticipated. As a next step, we also simulated a change of the membrane shape in time. To this end we allowed σ in Eq. 10 to perform a random walk in the interval $(-1, 1)$ with different ''diffusion'' constants, thereby interpolating between hyperbolic and parabolic surfaces. The resulting $C(\tau)$ is shown in Fig. 5 *c*. The curves not only decay slower than the simple expression Eq. 4, but also show a different decay behavior, which is reminiscent of the shapes observed for the hyperbolic manifolds. Again, a fractal analysis did not show any traces of anomalous diffusion, whereas $C(\tau)$ on the whole was well described by Eq. 7.

As another, more complicated surface with a different topology, we studied the *G* periodic nodal surface, defined by

$$0 = \sin(X)\cos(Z) + \sin(Y)\cos(X) + \sin(Z)\cos(Y), \quad (11)$$

where $X = 2\pi x/d_0$, $Y = 2\pi y/d_0$, $Z = 2\pi z/d_0$, and d_0 is the characteristic length between two nodes. This surface reminds in its topology of the ER of living cells (see Fig. 6, *inset*) and we therefore used it as a model for this membrane compartment. The FCS curve and its fractal analysis for this surface showed normal diffusive behavior as anticipated from the definition of the simulation (Fig. 6). However, the autocorrelation curve decays slower than expected for particles moving on a plane membrane, though the underestimation of the mobility is less strong than in the previous cases.

DISCUSSION

By subjecting the fluorescence signal $F(t)$ obtained in conventional FCS applications to a fractal analysis, we have shown that the fractal dimension D_0 of $F(t)$ is intimately connected to the degree α of anomalous diffusion. In particular, the behavior of the autocorrelation function $C(\tau)$ and the variance of fluorescence increments $v(\tau)$ is governed by power laws in the limit of small τ, where the exponent is simply given by α. Using this information, we could determine that GalNAc-T2(GFP), GalT(GFP), and p24β1(YFP) move subdiffusively in the ER and the Golgi apparatus with different degrees of anomality α. This seemed to be an inherent property of the protein rather than an effect

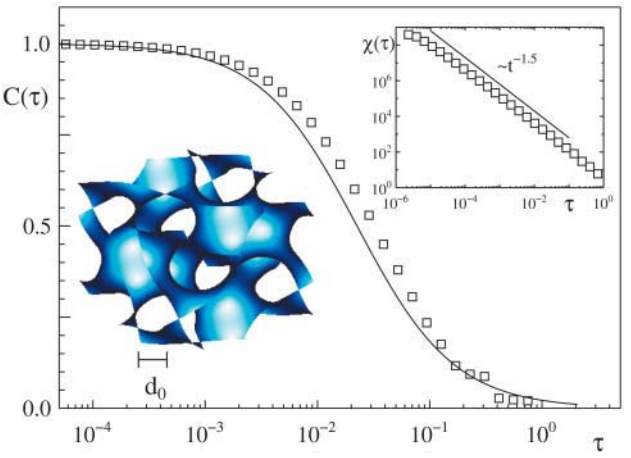

FIGURE 6 Autocorrelation curve $C(\tau)$ for FCS on the *G* periodic nodal surface (*inset lower left*, Eq. 11). The characteristic distance was chosen to be $d_0 = 0.2$ μm. The numerical data (*symbols*) decays 1.3-fold slower than theoretically expected (*full line*). As anticipated, the box-counting algorithm yields a scaling $\chi(\tau) \sim \tau^{-1.5}$ as required for normal diffusion (*inset upper right*). All times τ are in units of seconds.

of the particular environment. Using a simulation approach, we could rule out that the membrane shape induces anomalous diffusion, although it can change the apparent mobility by up to an order of magnitude.

Although anomalous diffusion could also, in principle, be detected by the asymptotic power-law decay $C(\tau) \sim \tau^{\alpha}$, $\tau^{\alpha}\Gamma \gg 4r_0^2$ when displaying $\log\{C(\tau)\}$ versus $\log\{\tau\}$, this approach is usually not feasible as it requires very long time series. About 3–4 orders of magnitude beyond $\tau^{\alpha}\Gamma \approx 4r_0^2$ with sufficient statistics are needed to enable this, i.e., typically a time series $F(t)$ of length $t_{max} > 1000$ s is required for statistical significance in the regime $\tau \leq 100$ s. While for giant liposomes these times may still be feasible, they are prohibitively long for in vivo applications when membranes are subject to movement and reformation, which perturbs the anticipated information. Also, the shape of the membrane can considerably influence the shape of $C(\tau)$ and mimic anomalous diffusion, although actually normal diffusion is observed. In contrast, our approach of analyzing the fractality of $F(t)$ on short timescales allows us to neglect the membrane curvature and yields a way to estimate if and to what degree anomalous diffusion plays a role in the FCS signal, even when $t_{max} \approx 10$ s. Our approach to estimate α requires a window of at least 1–2 orders of magnitude in τ to determine the involved power laws. We would like to stress that the range of fitting is very important for determining the proper value of α. An upper boundary for the fitting range is given by the restriction that the scaling $v(\tau) \sim \tau^{\alpha}$ can only be expected to hold true as long as $\Gamma\tau^{\alpha} \ll 4r_0^2$. The lower boundary is less well defined, but is essentially dictated by the conversion of fluorophores to the triplet state on time scales $\tau \leq 10$ μs. Our method is only applicable when the half time of $C(\tau)$ is at least 1–2 orders of magnitude bigger than this triplet time and if the fraction of molecules in the triplet state is low. As the fraction of dye molecules in the triplet state rises with the intensity of the laser light (Widengren, 2001), it is essential to use low powers. As anomalous diffusion typically yields $\Gamma\tau^{\alpha} = 4r_0^2$ for $\tau \approx 1$ ms in the nucleus of cells (Wachsmuth et al., 2000) and $\tau \approx 10$ ms on membranes (this study), one has under these conditions ~1–2 orders of magnitude for applying the fractal analysis. Our experimental data confirm this reasoning.

A possible source of error in our above analysis is the recently reported deviation of the confocal volume from the theoretically assumed Gaussian form (Hess and Webb, 2002). These deviations can lead to artifacts during the data evaluation when simply assuming a Gaussian volume. For example, the correlation function can mimic a two-component system even if only a single species is present. Likewise, $C(\tau)$ could also be fitted well by anomalous expressions such as Eq. 7 yielding $\alpha \approx 0.9$ (Hess and Webb, 2002), which is, however, considerably higher than the values found here (Fig. 3 *c*). To address concerns that our confocal volume is non-Gaussian, we have monitored the free diffusion of fluorescein isothiocyanate-labeled immunoglobulins (IgG) in buffer. Due to the high molecular weight of IgG, the diffusional decay of $C(\tau)$ is well separated from the triplet contribution on scales $\tau \ll 10$ μs (Widen-

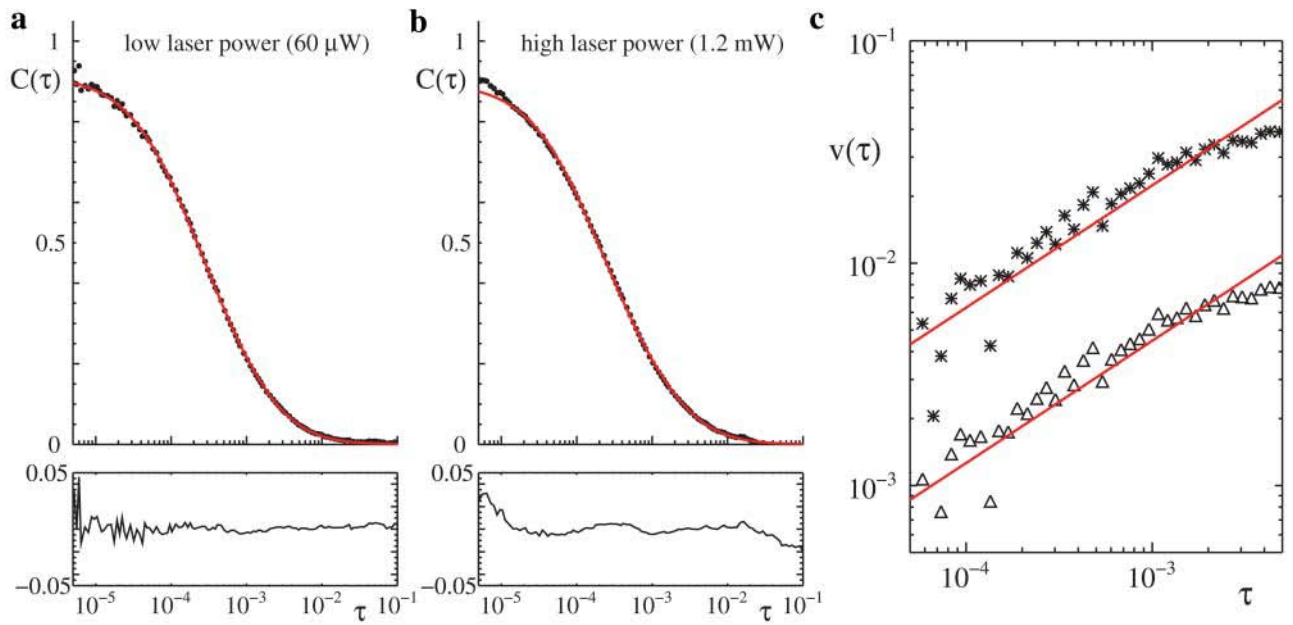

FIGURE 7 Autocorrelation curve $C(\tau)$ for fluorescein isothiocyanate-IgG (*symbols*) at (*a*) 60 μW and (*b*) 1.2 mW laser intensity. Whereas for low intensities the correlation decay is well fitted by the standard expression (*red line*), which assumes a Gaussian confocal volume, the residuals (*lower panel*) grow considerably for higher intensities, indicating a non-Gaussian confocal volume as reported in Hess and Webb (2002). (*c*) Changing the pinhole from one Airy unit (*triangles*) to two (*stars*) when performing FCS on GalT in vivo does not affect the scaling $v(\tau) \sim \tau^{0.55}$. All times τ are in units of seconds.

gren, 2001). We tested various laser powers and pinhole sizes, fitted $C(\tau)$ with an expression for diffusional motion in three dimensions (Rigler and Elson, 2001), and calculated the residuals. A representative curve for the conditions that were used in the live cell measurements is shown in Fig. 7 *a*. The extremely low residuals indicate that the confocal volume indeed is very well approximated by a Gaussian form. We therefore conclude that the deviations of the confocal volume from a Gaussian form do not play a major role in our measurements. We note that for higher laser powers, the residuals grow considerably (Fig. 7 *b*). We therefore recommend the use of low laser intensities also for this reason.

The observed deviations from a Gaussian confocal volume also limit the range over which the influence of the triplet kinetics can be studied while still keeping the confocal volume Gaussian. However, as the value of α stayed constant in all live cell measurements with laser intensities $40\ \mu\text{W} \le I \le 100\ \mu\text{W}$ (I changed from cell to cell depending on the expression level), the triplet kinetics does not seem to play a major role for our analysis. Also changing the pinhole did not affect α (see Fig. 7 *c* for an example).

We rule out the possibility that the anomalous decaying $C(\tau)$ could be due to multiple components with a peculiar distribution of diffusive times. Although theoretically possible, this problem is unlikely to play a role in this study: there exists a minimum diffusive time for an integral membrane protein that can be estimated via the Saffmann-Delbrück equation, i.e., $D \approx 2\ \mu\text{m}^2/\text{s} \Rightarrow \tau_D \approx 3$ ms. This represents a lower cutoff for the distribution of diffusive times, and if the motion of the proteins would not be anomalous, one should observe $v(\tau) \sim \tau$ for $\tau \ll 3$ ms. As the scaling $v(\tau) \sim \tau^{\alpha}$ is also observed on scales $\tau \ll 3$ ms (see Figs. 2 and 3), it is very unlikely that we have monitored multiple components with a peculiar distribution of diffusive times.

Finally, we would like to comment on the influence of the membrane shape on the estimate for the mobility of membrane proteins. As reported here, the apparent mobility can be changed by an order of magnitude depending on the local shape of the membrane. Similar observations have been made for FRAP applications (Aizenbud and Gershon, 1982). One may wonder if this uncertainty is in any way crucial. In fact, taking the Saffmann-Delbrück equation for the diffusion coefficient of membrane proteins (Saffman and Delbrück, 1975), one can infer that a factor of two in the mobility can correspond to a difference in size of the object by a factor of 10. If it is a cluster of proteins, this would correspond then to an assembly of ~200 monomeric proteins. In light of our findings, it will be interesting to revisit previous studies (Cole et al., 1996; Nehls et al., 2000) monitoring membrane protein dynamics in the ER and in the Golgi apparatus.

We thank P. Schwille (Max-Planck-Institute for Biophysical Chemistry, Göttingen, Germany), B. Storrie (Virginia Tech, Blacksburg, VA USA), T. Kottos (Max-Planck-Institute for Fluid Dynamics, Göttingen, Germany), and J. Young (European Molecular Biology Laboratory, Heidelberg, Germany) for helpful comments.

M.W. acknowledges financial support by a European Molecular Biology Organization long-term fellowship.

REFERENCES

Aizenbud, B. M., and N. D. Gershon. 1982. Diffusion of molecules on biological membranes of nonplanar form. A theoretical study. *Biophys. J.* 38:287–293.

Antonny, B., and R. Schekman. 2001. ER export: public transportation by the COPII coach. *Curr. Opin. Cell Biol.* 13:438–443.

Berry, M. V., and Z. V. Lewis. 1980. On the Weierstrass-Mandelbrot fractal function. *Proc. R. Soc. Lond. A.* 370:459–484.

Cole, N. B., C. L. Smith, N. Sciaky, M. Terasaki, M. Edidin, and J. Lippincott-Schwartz. 1996. Diffusional mobility of Golgi proteins in membranes of living cells. *Science.* 273:797–801.

Gennerich, A., and D. Schild. 2000. Fluorescence correlation spectroscopy in small cytosolic compartments depends critically on the diffusion model used. *Biophys. J.* 79:3294–3306.

Hess, S. T., and W. W. Webb. 2002. Focal volume optics and experimental artifacts in confocal fluorescence correlation spectroscopy. *Biophys. J.* 83:2300–2317.

Hołyst, R., D. Plewczyski, A. Aksimentiev, and K. Burdzy. 1999. Diffusion on curved, periodic surfaces. *Phys. Rev. E.* 60:302–307.

Hufnagel, L., R. Ketzmerick, and M. Weiss. 2001. Conductance Fluctuations of Generic Billiards: Fractal or Isolated? *Europhys. Lett.* 54:703–708.

Janowski, T., and R. Janka. 2001. ConfoCor 2, the second generation of fluorescence correlation microscopes. *In* Fluorescence Correlation Spectroscopy, Theory and Applications. R. Rigler and E. S. Elson, editors. Springer Series in Chemical Physics No. 65, Springer-Verlag, Heidelberg, 331–345.

Mandelbrot, B. B., and J. W. V. Ness. 1968. Fractional Brownian Motions, Fractional Noises and Applications. *SIAM Review.* 10:422–437.

Maspero, G., I. Guarneri, and G. Casati. 2000. Fractal survival probability fluctuations. *Phys. Rev. Lett.* 84:63–66.

Misner, C. W., K. S. Thorne, and J. A. Wheeler. 1973. Gravitation. Freeman, San Francisco.

Murray, J. D. 1993. Mathematical Biology, Biomathematics Texts, 2nd ed, Vol. 19. Springer-Verlag, Heidelberg, Germany.

Nagle, J. F. 1992. Long tail kinetics in biophysics? *Biophys. J.* 63:366–370.

Nehls, S., E. L. Snapp, N. B. Cole, K. J. Zaal, A. K. Kenworthy, T. H. Roberts, J. Ellenberg, J. F. Presley, E. Siggia, and J. Lippincott-Schwartz. 2000. Dynamics and retention of misfolded proteins in native ER membranes. *Nat. Cell Biol.* 2:288–295.

Nilsson, T., P. Slusarewicz, M. H. Hoe, and G. Warren. 1993. Kin recognition. A model for the retention of Golgi enzymes. *FEBS Lett.* 330:1–4.

Nilsson, T., M. H. Hoe, P. Slusarewicz, C. Rabouille, R. Watson, F. Hunte, G. Watzele, E. G. Berger, and G. Warren. 1994. Kin recognition between medial Golgi enzymes in HeLa cells. *EMBO J.* 13:562–574.

Rigler, R., and E. S. Elson, editors. 2001. Fluorescence Correlation Spectroscopy, Theory and Applications. Springer Series in Chemical Physics, No. 65, Springer-Verlag, Heidelberg, Germany.

Saffman, P. G., and M. Delbrück. 1975. Brownian motion in biological membranes. *Proc. Natl. Acad. Sci. USA.* 72:3111–3113.

Saxton, M. J. 2001. Anomalous subdiffusion in fluorescence photobleaching recovery: a Monte Carlo study. *Biophys. J.* 81:2226–2240.

Simons, K., and E. Ikonen. 2000. How cells handle cholesterol. *Science.* 290:1721–1726.

Schwille, P., J. Korlach, and W. W. Webb. 1999a. Fluorescence correlation spectroscopy with single-molecule sensitivity on cell and model membranes. *Cytometry*. 36:176–182.

Schwille, P., U. Haupts, S. Maiti, and W. W. Webb. 1999b. Molecular dynamics in living cells observed by fluorescence correlation spectroscopy with one- and two-photon excitation. *Biophys. J.* 77: 2251–2265.

Storrie, B., J. White, S. Röttger, E. H. Stelzer, T. Suganuma, and T. Nilsson. 1998. Recycling of golgi-resident glycosyltransferases through the ER reveals a novel pathway and provides an explanation for nocodazole-induced Golgi scattering. *J. Cell Biol.* 143:1505–1521.

Storrie, B., and T. Nilsson. 2002. The Golgi apparatus: balancing new with old. *Traffic*. 3:521–529.

Tatu, U., and A. Helenius. 1997. Interactions between newly synthesized glycoproteins, calnexin and a network of resident chaperones in the endoplasmic reticulum. *J. Cell Biol.* 136:555–565.

Wachsmuth, M., W. Waldeck, and J. Langowski. 2000. Anomalous diffusion of fluorescent probes inside living cell nuclei investigated by spatially-resolved fluorescence correlation spectroscopy. *J. Mol. Biol.* 298:677–689.

Widengren, J., 2001. Photophysical aspects of FCS measurements. *In* Fluorescence Correlation Spectroscopy, Theory and Applications. R. Rigler, and E. S. Elson, editors. Springer Series in Chemical Physics No. 65, Springer-Verlag, Heidelberg, 276–300.

Yamaguchi, N., and M. N. Fukuda. 1995. Golgi retention mechanism of beta-1,4-galactosyltransferase. Membrane-spanning domain-dependent homodimerization and association with alpha- and beta-tubulins. *Biol. Chem.* 270:12170–12176.